Supplementary Material (ESI) for Chemical Communications

Supporting Information

Low-Dimensional Chainlike Assemblies of TiO_2 Nanorod-Stabilized Au Nanoparticles

P. D. Cozzoli, E. Fanizza, M. L. Curri, D. Laub, A. Agostiano

1. Experimental details on the synthesis of the TiO_2 nanorod-stabilized Au nanoparticles

Materials. All chemicals were of the highest purity available and were used as received without further purification. Chloroauric acid trihydrate ($HAuCl_4{\cdot}3H_2O$, 99.998%), titanium tetraisopropoxide ($Ti(OPr^i)_4$ or TTIP, 99.999%), trimethylamino-N-oxide dihydrate ($(CH_3)_3NO{\cdot}2H_2O$ or TMAO, 98%), oleic acid ($C_{18}H_{33}CO_2H$ or OLEA, 90%) were purchased from Aldrich. All solvents used were of analytical grade and purchased from Aldrich.

Synthesis of TiO_2 nanorods. Organic-capped anatase TiO_2 nanocrystals were synthesized by hydrolysis of TTIP using OLEA as surfactant at low temperatures (80–100 °C), as reported elsewhere [a]. Briefly, TTIP was hydrolyzed by reacting with an excess of aqueous TMAO solution (H_2O:TTIP molar ratio ranged from 40:1 to 150:1). Rod-like titania nanocrystals resulted from direct injection of large aqueous base volumes into OLEA:TTIP mixtures. The as-prepared OLEA-coated TiO_2 nanoparticles were easily re-dispersed in chloroform, without any further growth or irreversible aggregation.

In the photocatalytic experiments in this work, the native organic capping on the titania nanocrystals was first removed by extensive washing, and then replaced by a fresh one as described in ref. 18 of the manuscript.

Photocatalytic synthesis of TiO_2/Au nanocomposites. A quartz cuvette was filled with a solution containing the desired concentration of TiO_2 nanocrystals (expressed with reference to the parent species, TTIP) and $HAuCl_4$ in a $CHCl_3$:EtOH mixture (EtOH content was 30% v/v to allow for the solubilization of $HAuCl_4$). $HAuCl_4$ concentration ranged between 10^{-5} M and 10^{-4} M, while TiO_2 concentration was between 10^{-3} M and 10^{-1} M. To obtain stable nanocomposite (i.e. to prevent the precipitation of the gold particles), the TiO_2:$HAuCl_4$ molar ratio should be kept in the range 100:1 to 20:1. The cuvette was sealed by a Teflon-faced rubber cap and the solution was subsequently deaerated by gently purging with nitrogen for 30 min. The mixture was UV-irradiated under stirring by using a High Pressure 200 W mercury lamp ($\lambda > 300$ nm). The lamp output was reduced to 10% of the original power by placing neutral density filters on the light path. This condition also ensured a minimal photo-oxidation of the TiO_2 organic capping, thereby prolonging the colloidal stability of the TiO_2 nanorods under illumination (see ref. 18 in the paper)

Aliquots were withdrawn at scheduled time intervals via a syringe for TEM investigations. The evolution of the surface plasmon absorption of gold was followed by taking the absorption spectrum of the extracted aliquots after exposing them to ambient atmosphere for ~2 min. Oxygen served to instantly scavenge the conduction band (CB) electrons which remained trapped on TiO_2 during photocatalysis in ethanolic media and which produced a weak blue colour [b–d] interfering with the optical features of gold. The deaerated TiO_2–$HAuCl_4$ reaction mixture exhibited such absorption contribution from TiO_2 accumulated CB electrons only after the metal ion reduction had gone to completion. Only after this stage on, the progressive assembly of the metal particles could be observed by TEM.

The final color of the aerated TiO_2–Au solution ranged from pale pink to dark red, to blue depending on the final size and aggregation status of the gold nanoparticles. The TiO_2–Au nanocomposite solutions remained stable under air for several weeks after preparation.

For a comparison, irradiation of TiO_2—$HAuCl_4$ solutions was also carried out by using the visible light of a 200 W quartz tungsten-halogen lamp (λ < 340 nm was cut by a suitable glass filter): in these cases, no formation of metallic gold was detected on a comparable time scale.

The necessity of UV-light to initiate efficient metal ion reduction pointed to the photocatalytic nature of the process involved in the formation of the metallic nanoparticles. Band-gap photoexcitation of titania by UV light provided reducing species for $HAuCl_4$, namely TiO_2 conduction band (CB) electrons (E^0 for e_{CB}^- is –0.5 V *vs.* NHE at pH 7) and $CH_3CH^{\bullet}OH$ radicals ($E^0{}_{1/2}$ for $CH_3CHO/CH_3CH^{\bullet}OH$ is –0.94 V *vs.* NHE) [f–g], these latter deriving from ethanol oxidation by the photogenerated valence band (VB) holes (E^0 for h_{VB}^+ is +2.7 V at pH 7 *vs.* NHE, $E^0{}_{1/2}$ for $CH_3CH^{\bullet}OH/C_2H_5OH$ is +1.13 V *vs.* NHE) [g]. Deaerated conditions prevented the reductants from being consumed by reacting with oxygen, while ethanol simultaneously served as hole scavenger. Such combined actions kept Au(III) reduction pathways dominant over Au(0) back-oxidation by the holes, thus allowing for the steady growth of the metal clusters. Hole scavenging also helped in preserving the TiO_2 surface organic-coating from photo-deterioration which could, in fact, lead to loss of colloidal stability for the metal particles through precipitation of the supporting nanorods. Similar findings are reported in ref. 18 of the manuscript.

2. Additional TEM characterization

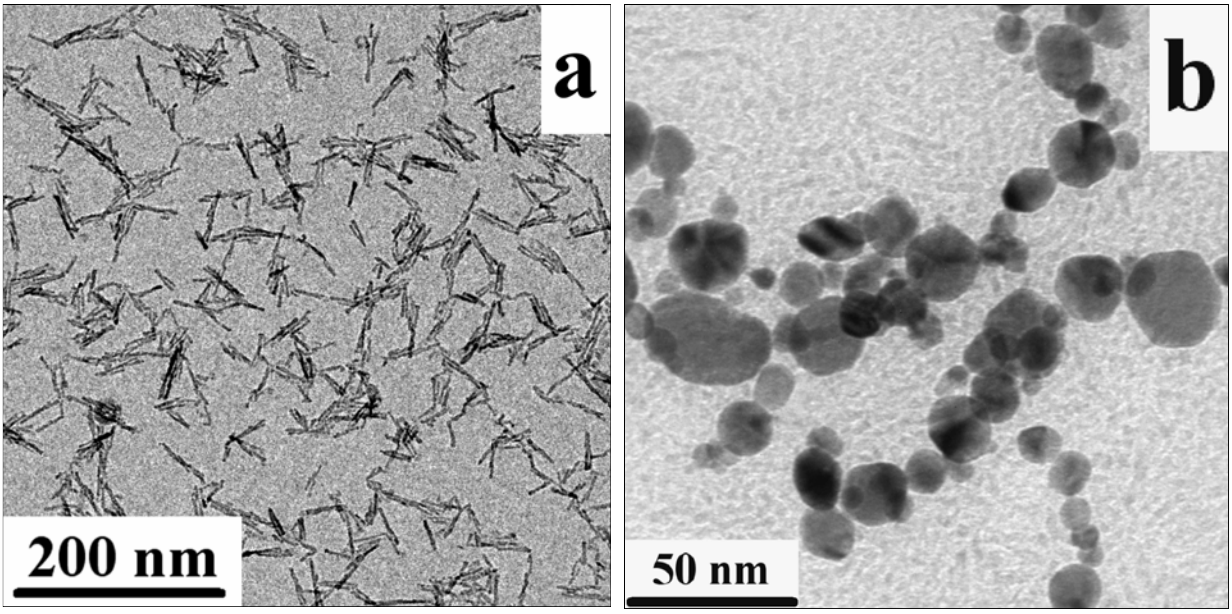

Figure 1S: Low resolution TEM images of (a) TiO_2 nanorods deposited from very diluted solutions of TiO_2 nanorods in $CHCl_3$; (b) typical gold nanoparticle chains deposited from TiO_2–Au nanocomposite solutions. Because of the significantly different image contrast characterizing TiO_2 when compared to Au, the gold nanoparticles can be easily identified as dark spots superimposed on an underlying titania background, as confirmed by energy dispersive analysis of X-rays (EDAX). Electron diffraction pattern analysis also reveals that the samples contain metallic gold and anatase titania. Due to the higher TiO_2 concentration used in the synthesis of the nanocomposites, in (b) the TiO_2 nanorods can not be individually discerned, as they form a dense film that covers entirely the carbon grid. The Au nanoparticles are thus embedded in such film. Detailed inspection of the Au assembled structures at higher magnification revealed that along each chain the component particles are always in contact with each other, either side by side or by partial superimposition. The particle do not coalesce or fuse, but retain their individuality, as demonstrated by the higher TEM contrast of areas corresponding to regions where two adjacent particles overlap. Interestingly, this observation in conjunction with the low contrast distinguishing especially the larger particles (see arrows in the figure) strongly suggests that many gold nanoparticles (~ 40% of the population) are flattened rather than spherical. The shape has been further verified by tilting the TEM sample plane from -45° through 0° to +45° (data not shown).

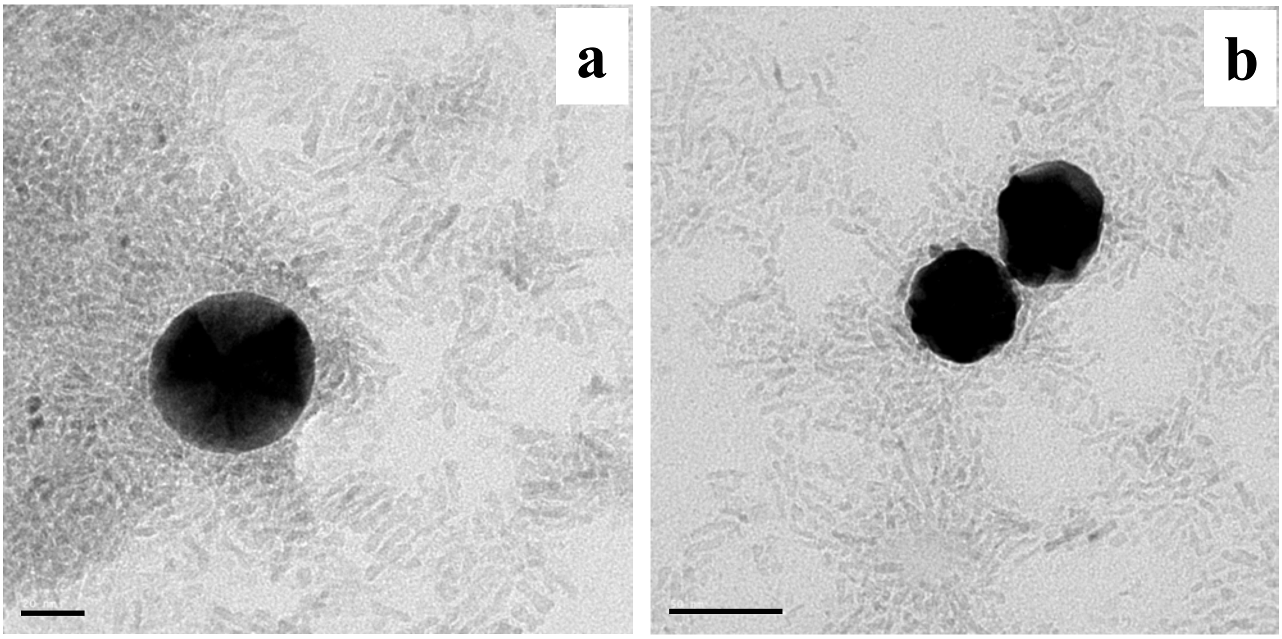

Figure 2S: High resolution TEM images showing characteristic assemblies of gold nanoparticles and TiO_2 nanorods. The TiO_2 nanorods could be observed in close contact to the Au nanoparticles even in samples deposited from highly diluted nanocomposite solutions and/or from solutions containing comparatively lower TiO_2 concentration. The scale bar is 20 nm in (a) and 50 nm in (b).

3. Colloidal stabilization of the Au nanoparticles by means of TiO_2 nanorods

As a general feature, the synthetic procedure always yielded optically clear mixtures of TiO_2 nanocrystals and individual gold nanoparticles. This result apparently differs from earlier preparations of oxide-supported gold [h–n] in which the metal ion reduction resulted in the deposition of small metallic islands on the oxide surface or in a discontinuous metal shell covering the oxide core. The mechanism for the colloidal stabilization of the gold nanoparticles was deduced by the following experiments.

1) Selective precipitation of the gold particles from stable nanocomposites was attempted by dropwise addition of a polar solvent (methanol or ethanol), according to conventional nonsolvent-based procedures to induce the precipitation of colloidal nanocrystals from nonpolar solutions. However, when the limit for the precipitation was reached (> 50% v/v EtOH or MeOH excess), a precipitate was collected by centrifugation which contained both gold and titania nanoparticles and that could be re-dispersed in $CHCl_3$.

2) The participation of the organic ligands desorbing from the surface of titania (*i.e.* OLEA) in the colloidal stabilization of gold clusters was investigated by carrying out $HAuCl_4$ photoreduction without TiO_2, but in presence of oleic acid at an OLEA:$HAuCl_4$ molar ratio in the range 1:1–20:1. Tetrabutylammonium borohydryde (TBABH), UV-photogenerated ketyl radicals in the presence of isopropanol and acetone [e], or UV-photogenerated electrons from an illuminated TiO_2 nanorod-thin film deposited onto a quartz substrate were alternatively employed as reductants to produce metallic particles. As a matter of fact, Au(III) reduction in the presence of the OLEA molecules yielded unstable colloidal metal particles that precipitated within a few hours or remained stuck onto the quartz cuvette walls.

In agreement with the mechanism previously found for silver (see ref. 18 in the paper), it can be suggested that steric hindrance posed by the surface OLEA ligands of titania prevented metal deposition directly onto the oxide nanorods. However, these latter could stabilize the Au nanoparticles growing in solution possibly through electrostatic or dipolar attractions, eventually enhanced at the ends of the nanorods because of the easier desorption of OLEA at these locations. The following observations supported this mechanism.

First, a minimum oxide support concentration was required to obtain optically clear TiO_2–Au nanocomposite solutions with long-term colloidal stability. Second, treatments aiming to the destabilization of the sole Au nanoparticles to obtain their selective extraction, based on the controlled addition of a non-solvent (MeOH or EtOH, > 50% v/v), determined the co-precipitation of the TiO_2 nanorods, thus proving the intimate interactions of titania with the metal. Third, the participation of oleic acid (OLEA) molecules desorbing from the surface of titania in the colloidal stabilization of Au clusters was excluded by carrying out $HAuCl_4$ reduction by other reductant systems in the presence of OLEA as the exclusive stabilizer. In these attempts, the amount of the employed surfactants was even far exceeding the total ligand content that could be found in the presence of the TiO_2 nanorods, where it was approximately dictated by the amount of organic stabilizers bound to the titania surface. It could be also assumed that the establishment of a reversible adsorption–desorption equilibrium of the ligands at the titania surface supplied only a negligible concentration of surfactant molecules in the bulk solution. As a matter of fact, without titania nanorods, no stable colloids were obtained, thus indicating that OLEA molecules did not bind strongly enough to the metal particle surface. Additionally, HRTEM investigations (see **Fig. 2S**) showed that the TiO_2 nanorods remained in close contact to the Au nanoparticles even in samples deposited from highly diluted nanocomposite solutions and/or from solutions containing low TiO_2 concentration.

All the above observations, taken together, suggested that the TiO_2 nanorods were actually responsible for the colloidal stabilization of the Au nanoparticles which could be therefore regarded as possessing virtually "bare" (*i.e.* not organic-passivated) surfaces.

4. Characterization techniques

*UV-vis Absorption spectroscopy***.** UV-vis absorption spectra were recorded with Cary 5 Varian UV-vis near-IR spectrophotometer.

Transmission Electron Microscopy. Transmission electron microscopy (TEM) images were obtained using Philips EM 430 microscope (TEM) operating at 300 kV. The samples for the analysis were prepared by dropping dilute solutions of freshly synthesized TiO_2–Au nanocomposite onto 400-mesh carbon-coated copper grids and leaving the solvent to dry. The samples were stable under the electron beam and did not degrade within the typical observation times. TEM samples were also prepared on grids with different coatings and by various rinsing and drying procedures to avoid artifacts due to solvent evaporation.

References

(a) Cozzoli, P. D.; Kornowski, A.; Weller, H. *J. Am. Chem. Soc.*, 2003, **125**, 14539.

(b) Kamat, P. V.; Bedja, I.; Hotchandani, S. *J. Phys. Chem.*, 1994, **98**, 9137.

(c) Vinodgopal, K.; Bedja, I.; Hotchandani, S.; Kamat, P. V. *Langmuir*, 1994, **10**, 1767.

(d) Safrany, A.; Gao, R.; Rabani, J. *J. Phys. Chem. B*, 2000, **104**, 5848.

(e) Henglein, A. *Chem. Mater.*, 1998, **10**, 444.

(f) Choi, W.; Hoffmann, M. R. *Environ. Sci. Technol.*, 1995, **29**, 1646.

(g) The potential is calculated from the polarographic half-wave potential, $E_{1/2} = -0.94$ V *vs.* NHE for the half-reaction of $CH_3CHO + e^- + H^+ \rightarrow CH_3CH^{\bullet}OH$ and $E^0 = +0.19$ V for the half-reaction of $CH_3CHO + 2e^- + 2H^+ \rightarrow C_2H_5OH$. See also ref. f.

(h) Kamat, P. V.; Flumiani, M.; Dawson, A. *Colloids Surf., A*, 2002, **202**, 269.

(i) Dawson, A.; Kamat, P. V. *J. Phys. Chem. B*, 2000, **104**, 11842.

(l) Subramanian, V.; Wolf, E. E.; Kamat, P. V. *Langmuir*, 2003, **19**, 469.

(m) Dawson, A.; Kamat, P. V. *J. Phys. Chem. B*, 2001, **105**, 960.

(n) Wood, A.; Giersig, M:, Mulvaney, P. *J. Phys. Chem. B*, 2001, **105**, 8810.